Redox interconversion between metal thiolate and disulfide compounds

Jiang, F.

Chapter 2

Redox Interconversion between Cobalt(III) Thiolate and Cobalt(II) Disulfide Compounds

The redox interconversion between Co(III) thiolate and Co(II) disulfide compounds has been investigated experimentally and computationally. Reactions of cobalt(II) salts with the disulfide ligand L^1SSL^1 (L^1SSL^1 = di-2-(bis(2-pyridylmethyl)amino)-ethyl disulfide) result in the formation of either the high-spin cobalt(II) disulfide compound $[Co^{II}_2(L^1SSL^1)Cl_4]$, or a low-spin, octahedral cobalt(III) thiolate compound, such as $[Co^{III}(L^1S)(MeCN)_2](BF_4)_2$. Addition of thiocyanate anions to a solution containing the latter compound yielded crystals of $[Co^{III}(L^1S)(NCS)_2]$. The addition of chloride ions to a solution of $[Co^{III}(L^1S)(MeCN)_2](BF_4)_2$ in acetonitrile results in conversion of the cobalt(III) thiolate compound to the cobalt(II) disulfide compound $[Co^{II}_2(L^1SSL^1)Cl_4]$, as monitored with UV-vis spectroscopy; subsequent addition of $AgBF_4$ regenerates the Co(III) compound. Computational studies show that exchange by a chloride anion of the coordinated acetonitrile molecule or thiocyanate anion in compounds $[Co^{III}(L^1S)(MeCN)_2]^{2+}$ and $[Co^{III}(L^1S)(NCS)_2]$ induces a change in the character of the highest occupied molecular orbitals, showing a decrease of the contribution of the p orbital on sulfur and an increase of the d orbital on cobalt. As a comparison, the synthesis of iron compounds was undertaken. X-ray crystallography revealed that structure of the dinuclear iron(II) disulfide compound $[Fe^{II}_2(L^1SSL^1)Cl_4]$ is different from that of the cobalt(II) compound $[Co^{II}_2(L^1SSL^1)Cl_4]$. In contrast to cobalt, reaction of the ligand L^1SSL^1 with $[Fe(MeCN)_6](BF_4)_2$ did not yield the expected Fe(III) thiolate compound. This work is an unprecedented example of redox interconversion between a high-spin Co(II) disulfide compound and a low-spin Co(III) thiolate compound triggered by the nature of the anion.

This chapter has been published as a full paper: Feng Jiang, Maxime A. Siegler, Xiaobo Sun, Lin Jiang, Célia Fonseca Guerra, and Elisabeth Bouwman, Inorg. Chem. 2018, 57, 8796-8805

2.1 Introduction

Sulfur-containing metalloenzymes are ubiquitous in biological systems and play fundamental roles in electron-transfer reactions including oxygen transport, nitrite reduction, and the synthesis of neurotransmitters [1-4]. A small number of these metalloenzymes involve thiolate/disulfide interconversion, related to the uptake or release of the metal ions [5-7]. For instance, copper delivery to the Cu_A site of cytochrome c oxidase (CcO) involves Sco proteins, and the potential operation principle has been suggested to involve thiolate/disulfide interconversion of two cysteine residues [8, 9]. Metallothionein Zn_7MT-3 has been reported to exchange its Zn(II) ions with Cu(II) centers of amyloid-β peptide (CuAβ). During this exchange four Cu(II) ions are reduced to Cu(I) by four cysteine thiolate groups in MT-3 with the formation of two disulfide bonds [10, 11]. The essence of the thiolate to disulfide oxidation of cysteines is an electron that shuttles from the cysteine thiolate sulfur to the metal ion in a high oxidation state, after which a disulfide is formed and a geometry change takes place of the reduced metal center in the active site. However, to the best of our knowledge, the exact mechanism is not well understood of this interconversion in biological systems [1]. In the last decades, this phenomenon inspired coordination chemists to synthesize metal thiolate compounds and study their redox interconversion. Since the first publication of a mixed-valence ($Cu^{II}Cu^{I}$) thiolate compound [12, 13], considerable efforts were put in the synthesis and characterization of Cu(II) thiolate compounds, and the investigation of their redox interconversion to the isomeric Cu(I) disulfide compounds [14-20]. The chloride-dependent redox interconversion between Cu(II) thiolate and Cu(I) disulfide compounds was first reported by Itoh et al. [20], followed later by the group of Henkel [15]. In recent years, our group further investigated the effect of temperature and solvents on the thiolate/disulfide redox interconversion of copper compounds [18]. Up until now, several triggers have been reported to influence the copper thiolate/disulfide redox interconversion like the addition of halide ions [15, 20] or protons [16, 19], as well as changes in temperature [18], and the polarity of solvents [18]. In addition, also ligand structure has a distinct influence on the redox interconversion (Scheme 2.1) [14, 21].

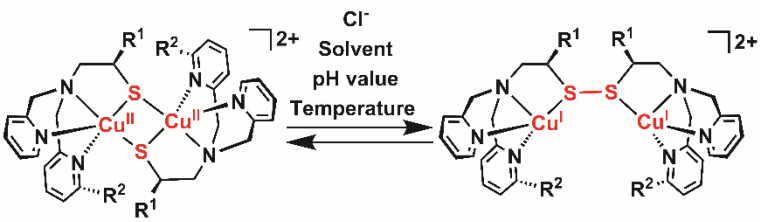

Scheme 2.1. Reported redox interconversion between copper(II) thiolate and copper(I) disulfide compounds triggered by different reaction conditions (R^1, R^2 = H, CH_3).

As electron-transfer reactions also take place in metalloenzymes containing metal centers other than copper [22, 23], all of this impressive work inspired us to study whether the thiolate/disulfide redox interconversion could occur for complexes of metal ions like cobalt or iron. Duboc et al. reported the electrochemical synthesis of a triplet-spin state (S = 1) Co(III) thiolate compound and its redox interconversion to a Co(II) disulfide compound triggered by the removal of chloride ions [24]. Herein, we report a low-spin (S = 0) Co(III) thiolate compound, which was formed directly from a reaction of a cobalt(II) salt with ligand di-2-(bis(2-pyridylmethyl)amino)-ethyl disulfide (L^1SSL^1). The redox interconversion of this Co(III) thiolate compound and the related Co(II) disulfide compound has been investigated. For comparison, the reaction of disulfide ligand L^1SSL^1 with iron(II) salts has been explored. This study not only provides a chemical perspective into the operation principle of electron transfer in metalloenzymes, but also extends the research on thiolate/disulfide interconversion to other metal centers.

2.2 Results

2.2.1 Synthesis and characterization of the cobalt and iron compounds

Ligand di-2-(bis(2-pyridylmethyl)amino)ethyl disulfide (L^1SSL^1) was synthesized using the reported procedure [20]. The coordination compounds were prepared following the procedure shown in Scheme 2.2. All the reactions were carried out under an oxygen-free atmosphere at room temperature, using standard Schlenk-line and glovebox techniques. Addition of 2 equiv of $CoCl_2{\cdot}6H_2O$ to ligand L^1SSL^1 dissolved in acetonitrile led to the formation of a purple solution, from which the compound $[Co^{II}_2(L^1SSL^1)Cl_4]$ (**1_{Co}**) was isolated in a yield of 64%. Addition of 2 equiv of $FeCl_2{\cdot}4H_2O$ to ligand L^1SSL^1 dissolved in methanol led to the formation of a greenish yellow solution, from which the compound $[Fe^{II}_2(L^1SSL^1)Cl_4]$ (**1_{Fe}**) was isolated in a yield of 62%. The addition of 2 equiv of $[Co(MeCN)_6](BF_4)_2$ to ligand L^1SSL^1 dissolved in acetonitrile resulted in a brown solution from which a compound with the assumed formula $[Co^{III}(L^1S)(MeCN)_2](BF_4)_2$ (**2**) was isolated as a brown oily material (in a yield

of 65%). Reaction of 2 equiv of $Co(NCS)_2$ with 1 equiv of ligand L^1SSL^1 dissolved in acetonitrile provided a brown precipitate of the Co(III) compound $[Co^{III}(L^1S)(NCS)_2]$ (**3**) in a yield of 70%. In contrast, reaction of 2 equiv of $[Fe(MeCN)_6](BF_4)_2$ with 1 equiv of ligand L^1SSL^1 dissolved in acetonitrile did not result in the anticipated Fe(III) thiolate compound but instead yielded a tetranuclear iron(II) fluoride compound [25]. The cobalt and iron compounds were characterized by using ^1H NMR, UV-vis, Raman, and IR spectroscopy, electrospray ionization mass spectrometry (ESI-MS), elemental analysis and single crystal X-ray crystallography.

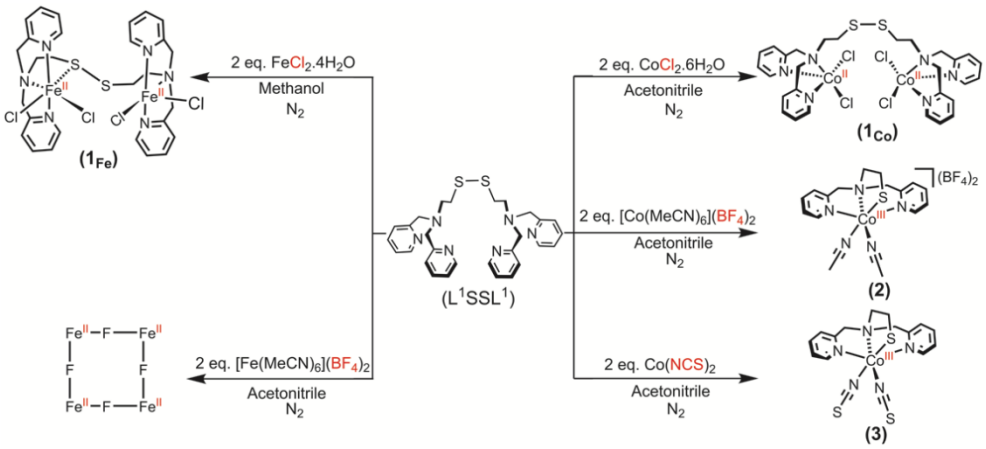

Scheme 2.2. Reactions of ligand L^1SSL^1 with different cobalt(II) and iron(II) salts.

ESI-MS spectra of purple compound $\mathbf{1_{Co}}$ dissolved in acetonitrile show a dominant peak (*m/z*) at 740.8 corresponding to the fragment $[Co^{II}_2(L^1SSL^1)Cl_3]^+$ (Figure AI.1). The ^1H NMR spectrum of the compound in dimethyl sulfoxide-d_6 shows broad resonances with shifts down to around 75 ppm (Figure AI.2), indicative of a paramagnetic compound. The effective magnetic moment of compound $\mathbf{1_{Co}}$ was estimated using Evans' method in dimethyl sulfoxide solution at 20 °C, revealing a μ_{eff} of 6.53 μ_B [26, 27]. This value is in agreement with two (weakly interacting) high-spin Co(II) centers (a value of 6.93 μ_B is expected for two isolated S = 3/2 cobalt(II) ions). ESI-MS spectra of compound $\mathbf{1_{Fe}}$ dissolved in methanol present a peak (*m/z)* at 349.1 corresponding to the dicationic species $[Fe^{II}_2(L^1SSL^1)Cl_2]^{2+}$ (Figure AI.3). The effective magnetic moment of $\mathbf{1_{Fe}}$ determined in methanol solution at 20 °C is in agreement with the presence of two high-spin Fe(II) centers in this compound (μ_{eff} = 7.67 μ_B; 8.94 μ_B is expected for two isolated S = 2 iron(II) centers). ESI-MS spectra of **2** dissolved in acetonitrile show a dominant peak (*m/z*) at 199.8 for the dicationic species $[Co^{III}(L^1S)(MeCN)_2]^{2+}$ (Figure AI.4). The ^1H NMR spectrum of brown compound **2** in acetonitrile-d_3 shows resonances in the diamagnetic region, consistent with the Co(III)

center in this compound being in a low-spin state (Figure AI.5). Similarly, the ^{1}H NMR spectrum of compound **3** in acetonitrile-d_3 shows resonances in the diamagnetic region (Figure AI.6). ESI-MS spectra of brown compound **3** dissolved in acetonitrile show a dominant peak (*m/z*) at 375.3 corresponding to the fragment $[Co^{III}(L^1S)(NCS)]^+$ (Figure AI.8).

Confocal Raman spectroscopy using a 476 nm laser was employed to study the disulfide bond in compounds $\mathbf{1_{Co}}$, $\mathbf{1_{Fe}}$, **2**, and disulfide ligand L^1SSL^1. The obtained spectra are provided in Figures AI.9 and AI.10. The Raman spectrum of ligand L^1SSL^1 shows clear bands at 522 and 550 cm^{-1}, which are attributed to the S-S bond vibration[28]. These bands are retained in the Raman spectra of $\mathbf{1_{Co}}$ and $\mathbf{1_{Fe}}$ and as expected are not present in the spectrum of **2**.

Attempts were undertaken to investigate the electrochemical properties of the cobalt compounds $\mathbf{1_{Co}}$, **2** and **3** using cyclic voltammetry in acetonitrile solutions with 0.1 M tetrabutylammonium hexafluoridophosphate as the supporting electrolyte (Figures AI.11–AI.14). Unfortunately, the compounds show multiple, poorly resolved redox waves, making it difficult to assign the various processes occurring in the solutions.

2.2.2 Description of the crystal structures

Single crystals of $\mathbf{1_{Co}}$ and **3** suitable for X-ray structure determination were obtained by vapor diffusion of diethyl ether and diisopropyl ether into acetonitrile solutions containing the compounds. Single crystals of $\mathbf{1_{Fe}}$ were grown by vapor diffusion of diethyl ether into a methanolic solution of the compound. Unfortunately, single crystals of **2** could not be obtained, but after 8 weeks from an acetonitrile solution of compound **2** kept in air, crystals were obtained of the cobalt(III) sulfinate compound $[Co^{III}(L^1SO_2)(MeCN)_2](BF_4)_2$ ($\mathbf{2_{Ox}}$). The crystal structure of $\mathbf{2_{Ox}}$ has been determined, and a projection of the structure is provided in Figure AI.15. Crystallographic and refinement data of the structures are provided in Table AI.1. A projection of the dinuclear structure of $\mathbf{1_{Co}}$ is shown in Figure 2.1a; relevant bond distances and angles are given in Tables 2.1 and 2.2. Compound $\mathbf{1_{Co}}$ crystallizes in the centrosymmetric space group $P\bar{1}$, with one dinuclear complex and one molecule of diethyl ether cocrystallized in the asymmetric unit. The two Co(II) ions are bound to three nitrogen atoms of the ligand and two chloride ions in distorted trigonal-bipyramidal geometries with the tertiary amine nitrogen and one of the chloride ions in the apical positions. The calculated τ values of the 5-coordinated geometries are 0.60 and 0.72 for Co1 and Co2, respectively. The τ value is determined from the two largest bond angles and is between 0 and 1, where 0 presents a perfect square-planar geometry, and 1 corresponds to an ideal trigonal-bipyramidal geometry [29]. The cobalt-to-

nitrogen bond lengths range from 2.064(2) to 2.311(2) Å. The sulfur atoms of the disulfide bond are noncoordinating; the Co-S distances are 5.9614(8) and 5.9371(7) Å. The distance between the two cobalt ions within the dinuclear structure is 8.1617(6) Å. Hydrogen-bond or stacking interactions are not present in this structure.

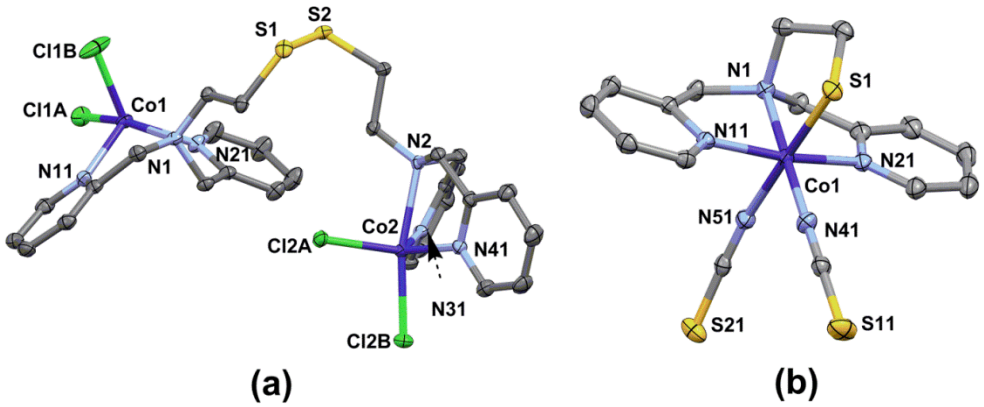

Figure 2.1. Displacement ellipsoid plots (50% probability level) of compounds (a) $[Co^{II}_2(L^1SSL^1)Cl_4]$ (**1**$_{Co}$) and (b) major component of $[Co^{III}(L^1S)(NCS)_2]$ (**3**) at 110(2) K. The lattice solvent molecule and hydrogen atoms are omitted for clarity. In the structure of **3**, partial oxidation of S1 was found (occupancy of the oxygen atom is 0.178(5)); a projection of the structure of the minor component is shown in Figure AI.16.

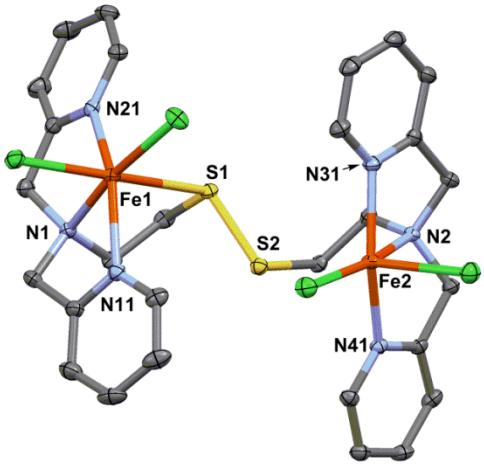

Figure 2.2. Displacement ellipsoid plots (50% probability level) of compound $[Fe^{II}_2(L^1SSL^1)Cl_4]$ (**1**$_{Fe}$) at 110(2) K. The lattice solvent molecule and hydrogen atoms are omitted for clarity.

A projection of the dinuclear structure of **1**$_{Fe}$ is shown in Figure 2.2; relevant bond distances and angles are presented in Table 2.3. Compound **1**$_{Fe}$ crystallizes in the

monoclinic space group *Cc*, with two lattice methanol solvent molecules in the asymmetric unit. The two Fe(II) centers in this dinuclear compound are in different geometries. Fe1 is in an octahedral geometry coordinated by two chloride ions, one thioether sulfur and three nitrogen donor atoms of the ligand. The three nitrogen donors are bound in a meridional fashion and the two chloride ions are in mutual *cis* positions, one of them *trans* to the thioether sulfur and the other *trans* to the tertiary amine. Fe2 is bound to two chloride ions and three nitrogen donors of the ligand in a pseudo-square-pyramidal geometry with a τ value of 0.25 [29]; also in this case the three nitrogen donors are bound in a meridional fashion in the equatorial plane of the square pyramid. The Fe1–S1 bond length is 2.6925(8) Å, which is much shorter than the Fe2–S2 distance of 3.231(1) Å, but longer than the Fe–S bond distances in some reported thioether-Fe(II) compounds (ranging from 2.200 to 2.285 Å) [30-32]. The Fe–N bond distances range from 2.135(2) to 2.270(3) Å for both Fe^{II} ions, in agreement with a high-spin state (S = 2) of both iron(II) centers. One of the two lattice methanol molecules is hydrogen bound to one of the coordinated chloride ions. The crystal packing of this structure shows no stacking interactions.

A projection of the mononuclear structure of **3** is shown in Figure 2.1b; relevant bond distances and angles are presented in Tables 2.1 and 2.2. Compound **3** crystallizes in the orthorhombic space group *Pbca*. The Co(III) ion is coordinated by three nitrogen donor atoms, one thiolate sulfur donor of the tetradentate ligand, and two nitrogen atoms of the thiocyanate anions in an octahedral geometry. The three nitrogen atoms of the tetradentate ligand are bound in a meridional fashion. The Co–S bond length is 2.2355(5) Å, the bond distances between the cobalt center and the five nitrogen donor atoms range from 1.9011(16) to 1.9934(15) Å. The thiocyanate donor atom N51 is at a significantly larger distance than N41, indicative of a larger *trans* influence of the thiolate sulfur donor. When finalizing the refinement, a residual electron density peak of 2.47 e^{-} $Å^{-3}$ was found at *ca.* 1.46 Å from S1. This peak is thought to arise from an oxygen atom, and its presence may result from the partial oxidation of S1 occurring during the crystallization process. Single crystals were obtained only after 3 weeks, during which time dioxygen must have diffused into the flask. Such a mono-oxygenated product likely is an intermediate in the oxidation of Co(III)-thiolate compound **2** to dioxygenated product $\mathbf{2_{ox}}$, containing a sulfinate ligand (Figure AI.15). A projection of the compound $[Co^{III}(L^{1}SO)(NCS)_2]$ (which is present with an occupancy factor of 0.178(5)) is given in Figure AI.16. Hydrogen-bond or stacking interactions are not present in this compound.

Table 2.1. Selected bond distances (Å) in the structures of compounds **1$_{Co}$** and **3**, as well as from the DFT-optimized structures of **1$_{Co}$**, **3**, cationic part of **2**, and the theoretical intermediates [Co^{III}(L^{1}S)(Cl)(NCS)] (**3a**), and [Co^{III}(L^{1}S)Cl$_2$] (**4**).[a]

	1Co		2	3		3a	4
Bond	**XRD**	**DFT**	**DFT**	**XRD**	**DFT**	**DFT**	**DFT**
Co1-N1	2.311(2)	2.392	1.942	1.9558(15)	1.947	1.947	1.950
Co1-N11	2.064(2)	2.061	1.932	1.9235(14)	1.922	1.916	1.918
Co1-N21	2.084(2)	2.057	1.932	1.9332(15)	1.924	1.917	1.923
Co1-S1	5.9614(8)	6.004	2.206	2.2355(5)	2.211	2.208	2.202
Co1-X1	2.3240(7)	2.330	1.857	1.9011(16)	1.855	1.851	2.261
Co1-X2	2.2716(8)	2.291	1.951	1.9934(15)	1.934	2.356	2.360

[a] X1 = Cl1A, X2 = Cl1B for **1$_{Co}$**; X1 = N41, X2 = N51 for **2** and **3**; X1 = N41, X2 = Cl1 for **3a**; X1 = Cl1A, X2 = Cl1B for **4**. All calculations were performed in the solvent.

Table 2.2. Selected bond angles (°) in the structures of **1$_{Co}$** and **3**.

1$_{Co}$		**3**			
Cl1A-Co1-Cl1B	100.76(3)	S1-Co1-N41	88.93(5)	N51-Co1-N11	88.17(6)
Cl1A-Co1-N1	169.92(6)	S1-Co1-N51	178.43(5)	N51-Co1-N21	91.59(6)
Cl1A-Co1-N11	102.96(6)	S1-Co1-N1	90.38(4)	N1-Co1-N11	84.32(6)
Cl1A-Co-N21	97.12(6)	S1-Co1-N11	92.10(4)	N1-Co1-N21	84.77(6)
Cl1B-Co1-N1	89.29(5)	S1-Co1-N21	88.44(4)	N11-Co1-N21	169.09(6)
Cl1B-Co1-N11	101.81(7)	N41-Co1-N51	89.50(6)		
Cl1B-Co1-N21	133.71(7)	N41-Co1-N1	179.31(7)		
N1-Co1-N11	75.42(8)	N41-Co1-N11	95.65(6)		
N1-Co1-N21	75.05(8)	N41-Co1-N21	95.26(7)		
N11-Co1-N21	115.20(9)	N51-Co1-N1	91.18(6)		

Table 2.3. Selected bond distances (Å) and angles (°) in the crystal structure of [Fe$^{II}_2$(L^{1}SSL^1)Cl$_4$] (**1$_{Fe}$**), as well as from DFT-optimized structures of the compound with different spin states (S = 2 and S = 0 for both iron centers).

Distances	**XRD**	**DFT** (S=2,2)	**DFT** (S=0,0)	**Angles**	**XRD**	**Angles**	**XRD**
Fe1-N1	2.270(2)	2.355	1.970	Cl1A-Fe1-Cl1B	100.40(3)	Cl2A-Fe2-Cl2B	101.45(3)
Fe1-N11	2.198(2)	2.129	1.942	Cl1A-Fe1-N1	93.12(6)	Cl2A-Fe2-N2	165.76(6)
Fe1-N21	2.187(2)	2.131	1.969	Cl1A-Fe1-N11	93.08(6)	Cl2A-Fe2-N31	103.69(7)
Fe1-S1	2.6925(8)	3.506	2.105	Cl1A-Fe1-N21	93.56(6)	Cl2A-Fe2-N41	102.55(6)
Fe1-Cl1A	2.4228(8)	2.415	2.413	Cl1B-Fe1-N1	166.05(6)	Cl2B-Fe2-N2	92.79(6)
Fe1-Cl1B	2.3419(7)	2.297	2.323	Cl1B-Fe1-N11	108.65(6)	Cl2B-Fe2-N31	94.52(6)
S1-S2	2.0576(9)	2.030	2.979	Cl1B-Fe1-N21	99.94(6)	Cl2B-Fe2-N41	93.26(6)
Fe2-N2	2.255(2)	2.355	1.969	N1-Fe1-N11	73.77(8)	N2-Fe2-N31	75.26(8)
Fe2-N31	2.141(2)	2.129	1.943	N1-Fe1-N21	75.57(8)	N2-Fe2-N41	75.98(8)
Fe2-N41	2.135(2)	2.132	1.968	N11-Fe1-N21	148.92(8)	N31-Fe2-N41	150.51(9)
Fe2-S2	3.231(1)	3.509	2.106	Cl1A-Fe1-S1	170.91(3)	S1-Fe1-N21	79.20(6)
Fe2-Cl2A	2.3035(8)	2.293	2.324	Cl1B-Fe1-S1	86.37(3)		
Fe2-Cl2B	2.4241(8)	2.416	2.414	S1-Fe1-N1	79.83(6)		
Fe1-Fe2	6.0567(6)	7.150	6.433	S1-Fe1-N11	90.45(6)		

2.2.3 UV-vis spectroscopy and reactivity

UV-vis spectra of purple **1$_{Co}$** dissolved in acetonitrile show four absorption bands (Figure 2.3a, black line). The absorption band at 261 nm (ε = 4.6×10^3 $M^{-1}cm^{-1}$) is

assigned to the π→π* transition of the pyridyl groups, whereas the three low-intensity bands at 524 (ε = 0.1×10³ $M^{-1}cm^{-1}$), 570 (ε = 0.1×10³ $M^{-1}cm^{-1}$), and 640 (ε = 0.1×10³ $M^{-1}cm^{-1}$) nm likely correspond to *d*–*d* transitions combined with a $Cl \rightarrow Co^{II}$ charge-transfer transition (LMCT) [33]. Absorption bands for the solid sample appear at 216, 253, 508, 595 and 797 nm (Figure AI.17). UV-vis spectra of brown compound **2** dissolved in acetonitrile reveal three absorption bands (Figure 2.3a, blue line). The band at 262 nm (ε = 8.1×10³ $M^{-1}cm^{-1}$) is ascribed to π→π* transition of the pyridyl groups, whereas the two absorption bands at 287 nm (ε = 6.9×10³ $M^{-1}cm^{-1}$) and 441 nm (ε = 0.4×10³ $M^{-1}cm^{-1}$) are tentatively ascribed to ligand-to-metal charge-transfer transitions (LMCT). UV-vis spectra of compound **3** dissolved in acetonitrile present four absorption bands (Figure AI.18). The absorption bands at 238 and 279 nm are assigned to the π→π* transitions of the pyridyl groups, whereas the two absorption bands at 325 and 515 nm likely correspond to LMCT transitions [33, 34]. The UV-vis spectrum of **3** in the solid state presents four absorption bands at 268, 336, 514, and 667 nm (Figure AI.19). UV-vis spectra of $\mathbf{1_{Fe}}$ dissolved in methanol show one strong absorption band at 256 nm (ε = 8.6×10³ $M^{-1}.cm^{-1}$) corresponding to the π→π* transition of pyridyl groups. In addition two weaker bands are observed at 313 nm (ε = 1.0×10³ $M^{-1}.cm^{-1}$) and 390 nm (ε = 1.8×10³ $M^{-1}.cm^{-1}$) tentatively ascribed to metal-to-ligand charge transfer (MLCT) transitions (Figure AI.20). The UV-vis spectrum of $\mathbf{1_{Fe}}$ in the solid state presents two bands: one at 256 nm and another broad band at around 353 nm (Figure AI.21).

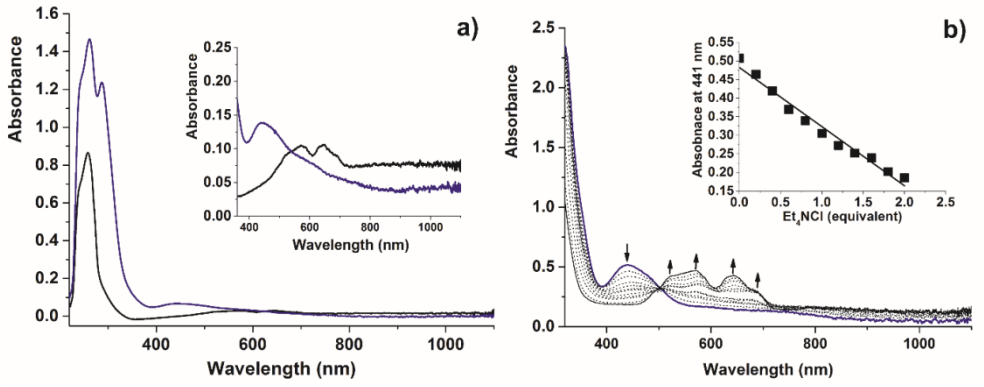

Figure 2.3. (a) UV-vis spectra of $\mathbf{1_{Co}}$ (black) and **2** (blue). UV-vis spectra were recorded using solutions 1 mM in [Co] with a transmission dip probe path length of 1.8 mm. The inset shows the UV-vis spectra of compounds recorded of solutions 2 mM in [Co]. (b) UV-vis spectra recorded upon addition of Et_4NCl to a solution of the compound $[Co^{III}(L^1S)(MeCN)_2](BF_4)_2$ (**2**) in acetonitrile. The spectra were recorded in at a concentration of 10 mM [Co] with a transmission dip probe path length of 2.3 mm. The inset shows the change of absorbance at 441 nm with addition of Et_4NCl.

To investigate the potential redox interconversion between the cobalt(II) disulfide compound and the cobalt(III) thiolate compound (Scheme 2.3), tetraethylammonium chloride was titrated into the acetonitrile solution containing Co(III) compound **2** while the reaction was monitored using UV-vis spectroscopy. The UV-vis spectra recorded during the addition of the chloride salt are shown in Figure 2.3b. With the addition of chloride ions into an acetonitrile solution of **2** the intensity of the absorption band at 441 nm gradually decreases until this band completely disappears after the addition of 2 equiv of chloride ion per cobalt center, while three new absorption bands appear at 524, 570, and 640 nm. The final spectrum equals the absorption spectrum of Co(II) compound $\mathbf{1_{Co}}$. Conversely, removal of chloride anions from Co(II) disulfide compound $\mathbf{1_{Co}}$ by titration with $AgBF_4$ leads to the regeneration of the Co^{III}–thiolate compound, as indicated by UV-vis spectroscopy (Figure AI.22).

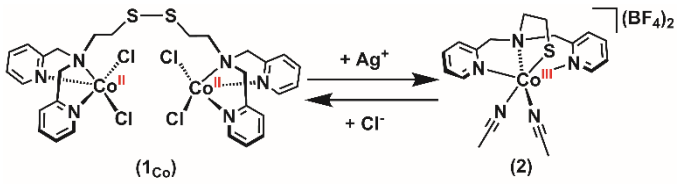

Scheme 2.3. Redox interconversion reaction of Co(II) compound $\mathbf{1_{Co}}$ and Co(III) compound **2** with the addition or removal of chloride anions.

The reaction of $\mathbf{1_{Fe}}$ with $AgBF_4$ in methanol solution was investigated as well, monitored by UV-vis spectroscopy under anaerobic conditions; the results are shown in Figure AI.23. With the addition of $AgBF_4$ the absorption at 313 nm decreases and fully disappears after addition of 4 equiv of $AgBF_4$, while the absorption band at 390 nm shifts to 368 nm. ESI-MS spectra of the final reaction mixture show the presence of a large number of species including a peak at *m/z* 734.8 for $[Fe_2(L^1SSL^1)Cl_3]^+$, indicating that the reaction does not simply yield the anticipated Fe(III) thiolate compound. As described above, the direct reaction of L^1SSL^1 with $[Fe(MeCN)_6](BF_4)_2$ yielded a tetranuclear Fe(II) compound of the disulfide ligand with bridging fluoride ions [25].

2.2.4 Computational characterization

To explore the electronic structures of $\mathbf{1_{Co}}$, $\mathbf{1_{Fe}}$, **2**, and **3** geometry optimizations were performed for all the compounds starting from the coordinates of the crystal structures. Quartet-spin (S = 3/2) and doublet-spin states (S = 1/2) of the Co(II) centers were considered for $\mathbf{1_{Co}}$. High-spin (S = 2) and low-spin (S = 0) states of iron(II) centers were taken into account for $\mathbf{1_{Fe}}$ and for the Co(III) center in the cationic parts of **2** and **3**. The obtained results are presented in Tables 2.1, 2.3, and Tables AI.3–AI.6

and Figures AI.24–AI.27 Comparison of the experimental and computed structures shows that the geometry of the cobalt centers in $\mathbf{1_{Co}}$ with quartet-spin states (two S = 3/2 ions) is more consistent with the crystallographic data. Furthermore, $\mathbf{1_{Co}}$ with quartet-spin states also has the lowest Gibbs free energy in the solvent, namely, 13 kcal/mol lower than for doublet-spin states (two S = 1/2 ions). The optimized (solvation) structure for $\mathbf{1_{Fe}}$ has the lowest Gibbs free energy with high-spin states ($\mathbf{1_{Fe}}_{(2,2,sol)}$, two S = 2 Fe^{II} centers), which is 31 and 10 kcal/mol lower than for the compound with two low-spin iron(II) centers ($\mathbf{1_{Fe}}_{(0,0,sol)}$, S = 0) and the compound with mixed-spin states ($\mathbf{1_{Fe}}_{(0,2,sol)}$, S = 0 for one iron(II) center and S = 2 for the other iron(II) center). The optimized geometry of $\mathbf{1_{Fe}}$ with two high-spin iron(II) centers is roughly similar to the crystallographic data; however, both Fe(II) ions are in a five-coordinate configuration, with Fe–S bond distances of 3.509 and 3.506 Å. For the optimized compound $\mathbf{1_{Fe}}_{(0,0\ sol)}$ in the low-spin state (S = 0 for both Fe^{II} ions), the S–S bond length is 2.979 Å, which is much longer than in the crystal structure of $\mathbf{1_{Fe}}$, whereas the Fe–S distances are much shorter than in the crystal structure. Therefore, as the computations did not reproduce the Fe–S distances, the geometry was optimized while keeping the distance between Fe2 and S2 fixed. The structure in the high-spin state ($\mathbf{1_{Fe}}_{(2,2,sol,fixation)}$, S = 2 for both Fe^{II} centers) still has the lowest Gibbs free energy and the acquired structure is consistent with the crystallographic data. Furthermore, the Gibbs free energy of $\mathbf{1_{Fe}}_{(2,2,sol,fixation)}$ is nearly the same as that of $\mathbf{1_{Fe}}_{(2,2,sol)}$. Apparently, the interaction between Fe2 and S2 is weak, and does not significantly affect the stability of the compound.

Both Co(III) compounds **2** and **3** have the lowest Gibbs free energy in the solvent with a low-spin Co(III) center, namely 25 and 23 kcal/mol lower than those with a high-spin Co(III) center. The selected bond lengths in the optimized structures of compounds **2** and **3** with the lowest energy are provided in Table 2.1. The Co–S bond lengths in the optimized structures of **2** and **3** are 2.206 and 2.211 Å, respectively, comparable to the Co–S bond length (2.2355(5) Å) found in the crystal structure of **3**. The calculations conducted in the gas phase show similar results with those in the solvent.

The addition of chloride anions to a solution containing cobalt(III)–thiolate compound **2** results in formation of cobalt(II)-disulfide compound $\mathbf{1_{Co}}$. To investigate this process computationally, the acetonitrile molecules in **2** and the thiocyanate anions in **3** were displaced by chloride ions one by one. The geometries of the theoretical intermediates $[Co^{III}(L^1S)(Cl)(MeCN)]^+$ (**2a**), $[Co^{III}(L^1S)(Cl)(NCS)]$ (**3a**), and $[Co^{III}(L^1S)Cl_2]$ (**4**) were optimized and their highest occupied molecular orbitals (HOMOs) were analyzed and compared with those of **2** and **3** (Scheme 2.4). The Gibbs free energies of the two

isomeric intermediates (with the chloride ion placed in the position *trans* to the amine nitrogen donor) are slightly higher than those of intermediates **2a** and **3a** (1 and 2 kcal/mol, respectively). This small difference may be caused by the trans influence of the thiolate donor, but this was not investigated in detail. Interestingly, the HOMOs of compounds **3**, **3a** and **4** consist mainly of *p* orbitals on sulfur and *d* orbitals on cobalt with the same total percentage (89% for all of the compounds). It was found that the HOMO gradually consists more of *d* orbital on cobalt and less of the *p* orbital of sulfur, as the number of chloride anions increases and the number of coordinated thiocyanate anions decreases. Similarly, displacement of the acetonitrile molecules in **2** by chloride anions effect the same change on HOMOs (Figure AI.28).

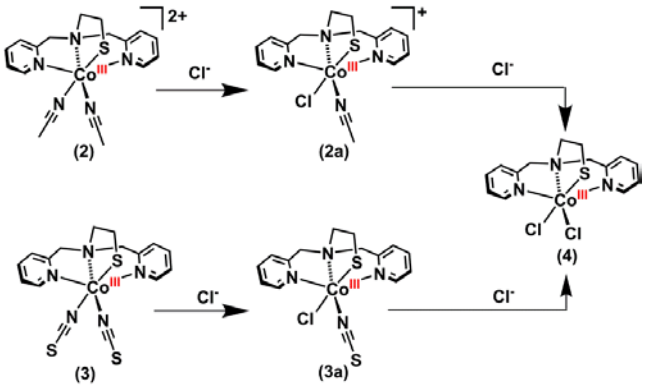

Scheme 2.4. Drawing of compounds **2**, **3**, and theoretical intermediates **2a**, **3a** and **4**.

It has been shown that depending on the experimental conditions dinuclear Cu(II) thiolate compounds $[Cu^{II}_2(L^1S)_2]^{2+}$ with bridging thiolate donor atoms may be generated when L^1SSL^1 or similar disulfide ligands react with Cu(I) salts [14, 18-20, 35]. However, mononuclear rather than dinuclear Co(III) thiolate compounds are formed in our study. In order to understand this difference in reactivity, both the hypothetical dinuclear compounds $[Co^{III}_2(L^1S)_2]^{4+}$ (**5**) and $[Co^{III}_2(L^1S)_2(MeCN)_2]^{4+}$ (**6**) with different spin states (S = 0, 1, or 2 for both Co(III) ions) were investigated computationally. As a comparison, the hypothetical mononuclear copper compound $[Cu^{II}(L^1S)(MeCN)]^{+}$ (**7**) and the actual dinuclear copper compound $[Cu^{II}_2(L^1S)_2]^{2+}$ (**8**) were optimized as well. The octahedral mononuclear copper(II) compound $[Cu^{II}(L^1S)(MeCN)_2]^{+}$ and the dinuclear copper(II) compound $[Cu^{II}_2(L^1S)_2(MeCN)_2]^{2+}$ have also been computed but are not discussed here as acetonitrile moved away from the Cu(II) center during the geometry optimization. The obtained results show that **5** has the lowest Gibbs free energy in the solvent with two low-spin cobalt(III) centers (two S = 0 ions); two high-spin states (two S = 2 ions) or two triplet-spin states (two S

= 1 ions) result in energies that are 40 and 3 kcal/mol higher. The energies of the antiferromagnetically coupled (S = 0) species were considered for the dinuclear copper(II) (two S = 1/2 ions) and cobalt(III) (two S = 2 ions in **5** or **6**, as well as two S = 1 ions in **5**) compounds (see Computational Details). Antiferromagnetic coupling (S = 0) is not beneficial to stabilize **5**, for S = 2 or S = 1 states result in Gibbs free energies being 29 and 24 kcal/mol higher than that of the uncoupled systems. The distance between two cobalt(III) ions in optimized geometries of **5** with two high-spin, two triplet-spin, two low-spin states are 3.665, 3.276, and 3.097 Å, respectively (Figure AI.29). Similarly, **6** with two S = 0 Co^{III} centers has the lowest Gibbs free energy in solvent. Optimization of **6** with two high-spin Co^{III} centers results in dissociation of the dinuclear structure (see Figure AI.30). Our computational study reveals that dimerization of mononuclear compound **2** to dinuclear compound **5** results in a slight decrease of the Gibbs free energy by 6 kcal/mol; however, formation of **6** leads to an increase of the Gibbs free energy by 19 kcal/mol (Figure 2.4). The formation of dinuclear copper compound **8** from mononuclear compound **7** leads to stabilization, lowering the Gibbs free energy by 33 kcal/mol (Figure 2.4, Tables AI.6 and AI.7).

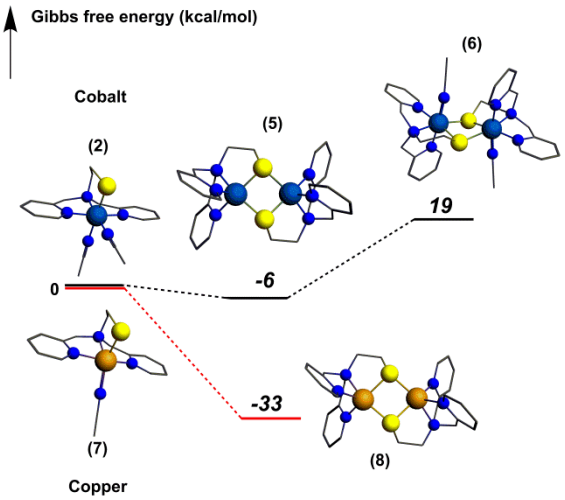

Figure 2.4. Optimized structures (at the the ZORA-OPBE/TZ2P level of theory) of compounds **2**, and **5–8**, and the change in Gibbs free energy (in kcal/mol) upon formation of the dinuclear metal compounds in acetonitrile. The acetonitrile molecules liberated in the reactions were taken into account but are omitted from the drawings for clarity.

2.3 Discussion

The redox interconversion between metal thiolate and disulfide compounds has received considerable attention in the past decade. In this chapter we report the synthesis of four new cobalt and iron compounds $[Co^{II}_2(L^1SSL^1)Cl_4]$ ($\mathbf{1_{Co}}$),

$[Fe^{II}_2(L^1SSL^1)Cl_4]$ (**1_{Fe}**), $[Co^{III}(L^1S)(MeCN)_2](BF_4)_2$ (**2**), and $[Co^{III}(L^1S)(NCS)_2]$ (**3**) from reactions of the disulfide ligand L^1SSL^1 with different Co(II) and Fe(II) salts. Whereas the Co(II) compounds are air-stable, the Co(III) thiolate compounds are slightly air-sensitive. The crystal structure of **3** showed the presence (with low occupancy factor) of a complex containing a mono-oxygenated sulfenate ligand, and crystallization of 2 in air after 8 weeks resulted in crystals of oxidized compound **2_{Ox}** comprising a dioxygenated sulfinate ligand. ESI-MS spectra of solutions containing **3** taken after 2 h in the air did not show any oxidation products, confirming that this oxidation process is very slow and thus that the effect on the redox studies is negligible. Using UV-vis spectroscopy, we showed that the addition of chloride anions to cobalt(III) compound **2** results in a redox interconversion reaction yielding cobalt(II) disulfide compound **1_{Co}**, whereas removal of the chloride anions from **1_{Co}** regenerates compound **2**. In 2001, the group of Itoh reported the synthesis of a Cu(II) thiolate compound from a similar disulfide ligand [20]. The addition of chloride anions to this Cu(II) thiolate compound led to the redox interconversion reaction to the corresponding Cu(I) disulfide compound, whereas removal of the chloride anions resulted in the regeneration of the Cu(II) thiolate compound. In contrast, the group of Henkel reported a Cu(I) disulfide compound that upon *addition* of chloride ions resulted in the formation of a Cu(II) thiolate compound [15]. Similarly, the group of Duboc recently reported a Co(III) thiolate compound that upon removal of chloride ions resulted in a Co(II) disulfide complex [24]. Clearly, the formation of metal thiolate or disulfide compounds cannot be predicted based on the anions only.

For comparison the synthesis of the related iron(II) compounds has been investigated. Reaction of ligand L^1SSL^1 with $FeCl_2{\cdot}4H_2O$ results in the formation of the iron(II) disulfide compound $[Fe^{II}_2(L^1SSL^1)Cl_4]$ (**1_{Fe}**), showing a structure that is slightly different from that of $[Co^{II}_2(L^1SSL^1)Cl_4]$ (**1_{Co}**). However, instead of the expected Fe(III)-thiolate compound similar to **2**, reaction of **1_{Fe}** with $AgBF_4$ did not give conclusive results, and reaction of ligand L^1SSL^1 with $[Fe(MeCN)_6](BF_4)_2$ resulted in the formation of a fluoride-bridged tetranuclear iron(II) compound [25]. Thus, the redox interconversion in the iron compound appears to be more difficult despite the fact that one of the thioether sulfurs in **1_{Fe}** is coordinating.

In order to understand the reactivity observed for our compounds, DFT calculations were employed to further explore the electronic structure of **1_{Co}**, **1_{Fe}**, **3**, and the cationic part of **2**. The obtained results show that **1_{Co}** has the lowest energy with two high-spin Co(II) centers (two $S = 3/2$ ions), consistent with the crystal structure and the observed effective magnetic moment, whereas low-spin Co(III) centers ($S = 0$) yield the lowest energy structures in compounds **2** and **3**, in agreement with the

crystal data and the diamagnetic NMR spectra. Similarly, $\mathbf{1_{Fe}}$ has the lowest energy with both iron centers in high-spin states (S = 2), in line with the crystal structure and the magnetic susceptibility in solution.

Combination of experimental results and DFT calculations confirm the formation of a low-spin (S = 0) mononuclear Co(III)-thiolate compound in contrast to the dinuclear dithiolate-bridged structure reported for Cu(II) and the dinuclear Co(II) compounds with quartet-spin state (two S = 3/2 ions) reported by the group of Duboc [18, 24]. The antiferromagnetic interaction between the two Cu(II) ions or the strong antiferromagnetic coupling between two S = 3/2 cobalt(II) ions reported by the group of Duboc are likely beneficial for the stabilization of the dinuclear compounds. Our computations show that antiferromagnetic coupling does not stabilize dinuclear cobalt(III) thiolate compounds **5** and **6**. Formation of dinuclear cobalt(III) compound **5** from mononuclear **2** seemingly results in a slightly lower Gibbs free energy, which suggests that in solution **2** and **5** may be in equilibrium. However, the compound that crystallizes from the solution is mononuclear **2**, and the question remains why the cobalt(III) ions in our ligand L^1S^- prefer a low-spin configuration in contrast to the intermediate spin occurring in the Duboc system.

The character of the HOMOs of compounds **2** and **3** and theoretical intermediates **2a**, **3a,** and **4** was investigated to explore the potential dependence of the electron distribution in the HOMO on the presence of different anions, as well as the potential transfer of electron density between cobalt and sulfur. The HOMO of these compounds has mainly character of *p* orbitals on sulfur and *d* orbitals on cobalt, and a small shift of the character of the HOMOs from *p* orbitals on sulfur to *d* orbitals on cobalt is found upon substitution of the thiocyanate by chloride anions. Our computational investigation on the potential shift of electron density from sulfur to cobalt upon coordination of chloride anions were not conclusive to help understand the experimental finding of the formation of a Co(II) disulfide compound upon addition of chloride ions.

2.4 Summary and conclusions

In this chapter, we report the synthesis of low-spin mononuclear Co(III) thiolate compounds and high-spin dinuclear Co(II) and Fe(II) disulfide compounds from a disulfide ligand L^1SSL^1 in reaction with Co(II) and Fe(II) salts. It is shown that the redox interconversion of this Co(III) thiolate and the corresponding Co(II) disulfide compound is triggered by the addition or removal of chloride anions. DFT calculations show that the HOMO consists gradually more of the *d* orbital on cobalt and less of the *p* orbital on sulfur when the thiocyanate molecules in the compound $[Co^{III}(L^1S)(NCS)_2]$

are substituted with chloride ions. This is the first example of a redox interconversion reaction between low-spin Co(III) thiolate and high-spin Co(II) disulfide compounds. Despite the new information that is gained including our computational studies, still more research needs to be done to predict accurately the conditions that trigger the redox interconversion reactions for metal thiolate and disulfide compounds.

2.5 Experimental section

2.5.1 General procedures

All the reagents were purchased from commercial sources and used as received unless noted otherwise. Dry acetonitrile and diethyl ether were obtained from a solvent dispenser (PureSolV 400), and methanol was acquired from commercial vendors and stored on 3 Å molecular sieves. The synthesis of metal compounds was carried out using standard Schlenk-line techniques under a nitrogen atmosphere. ^{1}H NMR spectra were recorded on a Bruker 300 DPX spectrometer at room temperature. Mass spectra were recorded on a Finnigan Aqua mass spectrometer with electrospray ionization (ESI). IR spectra were acquired on a PerkinElmer UATR spectrum equipped with a single reflection diamond (scan range 400 cm^{-1} to 4000 cm^{-1}, resolution 4 cm^{-1}). UV-vis spectra were collected using a transmission dip probe with variable path lengths and reflection probe on an Avantes Avaspec-2048 spectrometer with Avalight-DH-S-BAL light source. A WITEC alpha300R-Confocal Raman Imaging with the laser wavelength of 476 nm was used to record the Raman spectra, and all of the measurements were carried out under ambient conditions at room temperature. Elemental analyses were performed by the Microanalytical Laboratory Kolbe in Germany. Cyclic voltammetry (CV) was performed with an Autolab PGstat10 potentiostat controlled by GPES4 software. A three-electrode system was used including an Ag/AgCl double junction reference electrode, a glassy carbon working electrode (3 mm diameter), and a Pt wire counter electrode in a solution containing 0.1 M NBu_4PF_6. In these conditions the Fc/Fc^+ couple was found to be located at +0.428 V with a peak-to-peak separation of 91 mV in acetonitrile. Potentials are given relative to the Ag/AgCl electrode.

2.5.2 Single crystal X-ray crystallography

All reflection intensities were measured at 110(2) K using a SuperNova diffractometer (equipped with Atlas detector) with Mo Kα radiation (λ = 0.71073 Å) under the program CrysAlisPro (version 1.171.36.32 Agilent Technologies, 2013 was used for $\mathbf{1_{Co}}$, $\mathbf{2_{Ox}}$ and $\mathbf{1_{Fe}}$; version CrysAlisPro 1.171.39.29c, Rigaku OD, 2017 was used for compound **3**). The same program was used to refine the cell dimensions and for data reduction. The structures were solved with the program SHELXS-2013 or SHELXS-

2014/7 and were refined on F^2 with SHELXL-2013 or SHELXS-2014/7 [36]. Analytical numeric absorption correction based on a multifaceted crystal model or numerical absorption correction based on Gaussian integration over a multifaceted crystal model were applied using CrysAlisPro. The temperature of the data collection was controlled using the system Cryojet (manufactured by Oxford Instruments). The H atoms were placed at calculated positions using the instructions AFIX 23, AFIX 43 or AFIX 137 with isotropic displacement parameters having values 1.2 or 1.5 U_{eq} of the attached C atoms. The H atoms attached to O1S and O2S (lattice methanol solvent molecules) for $\mathbf{1_{Fe}}$ were found from difference Fourier maps, and their coordinates were refined freely. The structures of $\mathbf{1_{Co}}$, $\mathbf{2_{Ox}}$, $\mathbf{1_{Fe}}$ and **3** are mostly ordered.

For $\mathbf{1_{Fe}}$, the absolute configuration was established by anomalous-dispersion effects in diffraction measurements on the crystal, and the Flack and Hooft parameters refine to 0.006(5) and 0.010(6), respectively. While finalizing the refinement of **3**, one residual electron density peak of 2.47 e^- $Å^{-3}$ was found at *ca.* 1.46 Å from S1. This peak is thought to be an oxygen atom, and its presence may result from the partial oxidation of S1 occurring during the crystallization process. Its occupancy factor was set to refine freely, and its final value is 0.178(5). Another peak of 0.42 e^- $Å^{-3}$ was found at *ca.* 1.12 Å from S1. The nature of this peak is not entirely clear.

2.5.3 Density functional theory (DFT) calculations

All calculations were performed with the Amsterdam Density Functional (ADF) program version r47953 [37, 38], using relativistic DFT at ZORA OPBE/TZ2P for geometry optimization and energies.[39] Solvation in acetonitrile was simulated using the conductor-like screening model (COSMO) [40-43]. All stationary points in the gas phase and in the condensed phase were verified to be minima on the potential energy surface (PES) through vibrational analysis. The energies of the singlet state of the Cu^{II}/Co^{III} μ-thiolate complexes (E^S) have been obtained from the unrestricted broken-symmetry singlet energies (E^{BS}) and the energy of the triplet (E^T) with the approximate projection method of Noodleman: $E^S = 2E^{BS} - E^T$.[44, 45]

The Gibbs free energies ($\Delta G = \Delta H - T\Delta S$) were evaluated with the following procedure. Enthalpies at 298.15 K and 1 atm (ΔH_{298}) were calculated from electronic bond energies (ΔE) in the solvent and vibrational frequencies using standard thermochemistry relations for an ideal gas, according to [46]

$$\Delta H_{298} = \Delta E + \Delta E_{trans,298} + \Delta E_{rot,298} + \Delta E_{vib,0} + \Delta(\Delta E_{vib,0})_{298} + \Delta(pV) \quad (1)$$

Here, $\Delta E_{trans,298}$, $\Delta E_{rot,298}$, and $\Delta E_{vib,0}$ are the differences between the two complexes in translational, rotational and zero-point vibrational energy, respectively; $\Delta(\Delta E_{vib,0})_{298}$ is

the change in the vibrational energy difference as one goes from 0 to 298.15 K. The vibrational energy corrections are based on our frequency calculations in the gas phase. The molar work term $\Delta(pV)$ is (Δn)RT, with n=0. Thermal corrections for the electronic energy are neglected. The entropy ΔS was also obtained from the gas phase calculations. Most systems were optimized in C_1 symmetry. CH_3CN was optimized with C_{3v} symmetry.

2.5.4 Synthesis of the compounds

$[Co^{II}_2(L^1SSL^1)Cl_4]$ (**1_{Co}**): Ligand L^1SSL^1 (107.0 mg, 0.207 mmol) was dissolved in 3 mL of dry acetonitrile, and separately $CoCl_2{\cdot}6H_2O$ (98.5 mg, 0.414 mmol) was dissolved in 3 mL of dry acetonitrile. The two solutions were mixed resulting in a purple solution, which was stirred for about 30 min. Then, 8 mL of diethyl ether was added, and a purple precipitate was obtained which was washed with diethyl ether (5 × 5 mL). Yield: 99.1 mg, 0.13 mmol, 64%. Single crystals suitable for X-ray diffraction were obtained by slow vapor diffusion of diethyl ether into the acetonitrile solution containing the compound; single crystals were obtained after 2 days at room temperature. IR (cm^{-1}): 1606s, 1571w, 1480m, 1442s, 1092w, 1022m, 766vs, 648m, 478w. ESI-MS found (calcd) for $[M-Cl]^+$ *m/z* 740.8 (740.9). Elemental analysis calcd (%) for $C_{28}H_{32}Cl_4Co_2N_6S_2$+$2H_2O$: C 41.40, H 4.47, N 10.3; found: C 41.71, H 4.57, N 9.80. UV-vis (acetonitrile at 1 mM [Co]): λ_{max} (ε in M^{-1} cm^{-1}): 261 nm (4.6×10^3), 524 nm (0.1×10^3), 570 nm (0.1×10^3), 640 nm (0.1×10^3).

$[Co^{III}(L^1S)(MeCN)_2](BF_4)_2$ (**2**): To a yellow solution of ligand L^1SSL^1 (71.2 mg, 0.138 mmol) in 4.6 mL of dry and degassed acetonitrile, solid $[Co(MeCN)_6](BF_4)_2$ (131.7 mg, 0.275 mmol) was added, resulting in a brown yellow solution. The acquired solution was stirred for 3 h, and then the volume was reduced to 0.5 mL. Addition of 15 mL of diethyl ether led to the formation of a yellow oil material. The obtained yellow oil material was washed with diethyl ether (3 × 15 mL). Yield: 103.0 mg, 0.18 mmol, 65%. Single crystals of **2** could not be obtained, but from an acetonitrile solution of compound **2** kept in air, after 8 weeks crystals were obtained of the cobalt(III) sulfinate compound $[Co^{III}(L^1SO_2)(MeCN)_2](BF_4)_2$ (**2_{ox}**). IR (cm^{-1}): 1606m, 1481w, 1480w, 1444w, 1292m, 1018s, 764s, 727w, 648w, 523w, 476w. ^1H NMR (300 MHz, acetonitrile-d_3, RT): δ = 8.39 (2H, Py-H_6), 8.10 (2H, Py-H_4), 7.56 (4H, Py–H_3, Py–H5), 5.02 (2H, Py–CH_2), 4.34 (2H, Py–CH_2), 3.12 (N–CH2–CH2–S), 2.55 (proton probably from the coordinated acetonitrile), 2.09 (H_2O), 1.94 (MeCN). ESI-MS found (calcd) for ½ $[M-2(BF_4)]^{2+}$ *m/z* 199.8 (199.5). UV-vis (acetonitrile at 1 mM [Co]): λ_{max} (ε in M^{-1} cm^{-1}): 262 nm (8.1×10^3), 287 nm (6.9×10^3), 442 nm (0.4×10^3).

[$Co^{III}(L^1S)(NCS)_2$] (**3**): Ligand L^1SSL^1 (103.9 mg, 0.201 mmol) was dissolved in 5 mL of dry and degassed acetonitrile, to which solid $Co(NCS)_2$ (70.3 mg, 0.401 mmol) was added, resulting in a dark brown solution. The solution was stirred for 3 h at room temperature, after which the volume was reduced to 2 mL. Addition of 20 mL of diethyl ether resulted in the formation of a dark brown powder. The acquired powder was washed with diethyl ether (3 × 10 mL). Yield: 120.0 mg, 0.28 mmol, 70%. Single crystals suitable for X-ray diffraction were grown by slow vapor diffusion of isopropyl ether into the acetonitrile solution containing the compound; single crystals were obtained after approximately 3 weeks at room temperature. ^{1}H NMR (300 MHz, acetonitrile-d_3, RT): δ = 8.42 (d, 2H, Py-H_6), 8.01 (t, 2H, Py–H_4), 7.59 (t, 2H, Py–H_3), 7.45 (d, 2H, Py–H_5), 4.98 (d, 2H, Py–CH_2), 4.22 (d, 2H, Py–CH_2), 3.65 (d, 2H, S–CH_2–CH_2), 2.95 (t, 2H, S–CH_2–CH_2), 2.14 (H_2O), 1.94 (MeCN). ^{13}C NMR (300 MHz, acetonitrile–d_3, RT): δ = 30.67 (C–S), 67.95 (Py–C–N), 70.82 (N–*C*H2–CH_2–S), 121.88 (Py–C_5), 125.60 (Py–C_3), 139.66 (Py–C_4), 152.37 (Py–C_6), 162.11 (Py–C_2). ESI-MS found (calcd) for [M–NCS]$^+$ *m/z* 375.3 (375.1). IR (cm^{-1}): 2106vs, 2090s, 1608m, 1478m, 1445s, 1304m, 1277m, 1229w, 1156w, 1108w, 1054m, 1017w, 993w, 952m, 895m, 821m, 752vs, 786s, 652m, 557w, 532m, 479s. Elemental analysis calcd (%) for $C_{16}H_{16}CoN_5S_3$: C 44.34, H 3.72, N 16.16; found: C 44.19, H 3.87, N 15.94. UV-vis (acetonitrile at 1 mM [Co]): λ_{max} (ε in M^{-1} cm^{-1}): 238 nm (6.7×10^3), 279 nm (8.5×10^3), 325 nm (4.8×10^3), 515 nm (0.7×10^3).

[$Fe^{II}_2(L^1SSL^1)Cl_4$] (**$\mathbf{1_{Fe}}$**): Ligand L^1SSL^1 (77.7 mg, 0.150 mmol) was dissolved in 6 mL of dry and degassed methanol to which 60.0 mg (0.30 mmol) $FeCl_2{\cdot}4H_2O$ was added, resulting in a green-yellow solution. The solution was stirred for another 2 h at room temperature, after which 20 mL of dry and degassed diethyl ether was added, yielding a yellow precipitate. The obtained precipitate was filtered and washed with diethyl ether (4 × 15 mL). Yield: 59.3 mg, 0.07 mmol, 62%. Single crystals suitable for X-ray structure determination were grown by slow vapor diffusion of diethyl ether into a methanol solution of this compound; single crystals were obtained after 4 days at room temperature. IR (cm^{-1}):1604s, 1571w, 1479w, 1442s, 1291w, 1155w, 1088m, 1052m, 1019s, 764vs, 725w, 642w. ESI-MS found (calcd) for 1/2[M–2Cl]$^{2+}$ *m/z* 349.1 (349.0). Elemental analysis calcd (%) for $C_{28}H_{32}Cl_4Fe_2N_6S_2$+3$H_2O$: C 40.80, H 4.65, N 10.20; found: C 40.32, H 4.32, N 9.87. UV-vis (methanol at 1 mM [Fe]): λ_{max} (ε in M^{-1} cm^{-1}): 256 nm (8.6×10^3), 313 nm (1.0×10^3), 390 nm (1.8×10^3).

2.6 References

[1] C. Jacob, G.L. Giles, N.M. Giles, H. Sies, Angew. Chem., Int. Ed., 42 (2003) 4742-4758.
[2] S. Iwata, C. Ostermeier, B. Ludwig, H. Michel, Nature, 376 (1995) 660-669.

[3] J.A. Kovacs, Acc. Chem. Res., 48 (2015) 2744-2753.
[4] C.E. Paulsen, K.S. Carroll, Chem. Rev., 113 (2013) 4633-4679.
[5] A.L. Lamb, A.S. Torres, T.V. O'Halloran, A.C. Rosenzweig, Nat. Struct. Mol. Biol., 8 (2001) 751-755.
[6] P. Palumaa, L. Kangur, A. Voronova, R. Sillard, Biochem. J., 382 (2004) 307-314.
[7] E.S. Arnér, A. Holmgren, FEBS J., 267 (2000) 6102-6109.
[8] L. Banci, I. Bertini, G. Cavallaro, S. Ciofi-Baffoni, FEBS J., 278 (2011) 2244-2262.
[9] T.R. Cawthorn, B.E. Poulsen, D.E. Davidson, D. Andrews, B.C. Hill, Biochemistry, 48 (2009) 4448-4454.
[10] G. Meloni, V. Sonois, T. Delaine, L. Guilloreau, A. Gillet, J. Teissié, P. Faller, M. Vašák, Nat. Chem. Biol., 4 (2008) 366-372.
[11] J.T. Pedersen, C. Hureau, L. Hemmingsen, N.H. Heegaard, J. Østergaard, M. Vašák, P. Faller, Biochemistry, 51 (2012) 1697-1706.
[12] R.P. Houser, V.G. Young, W.B. Tolman, J. Am. Chem. Soc., 118 (1996) 2101-2102.
[13] R.P. Houser, J.A. Halfen, V.G. Young Jr, N.J. Blackburn, W.B. Tolman, J. Am. Chem. Soc., 117 (1995) 10745-10746.
[14] S. Itoh, M. Nagagawa, S. Fukuzumi, J. Am. Chem. Soc., 123 (2001) 4087-4088.
[15] A. Neuba, R. Haase, W. Meyer-Klaucke, U. Flörke, G. Henkel, Angew. Chem. Int. Ed., 51 (2012) 1714-1718.
[16] E. C.M. Ording-Wenker, M. van der Plas, M.A. Siegler, C. Fonseca Guerra, E. Bouwman, Chem. Eur. J., 20 (2014) 16913-16921.
[17] E.C.M. Ording-Wenker, M.A. Siegler, E. Bouwman, Inorg. Chim. Acta, 428 (2015) 193-202.
[18] E.C.M. Ording-Wenker, M. van der Plas, M.A. Siegler, S. Bonnet, F.M. Bickelhaupt, C. Fonseca Guerra, E. Bouwman, Inorg. Chem., 53 (2014) 8494-8504.
[19] A.M. Thomas, B.L. Lin, E.C. Wasinger, T.D.P. Stack, J. Am. Chem. Soc., 135 (2013) 18912-18919.
[20] Y. Ueno, Y. Tachi, S. Itoh, J. Am. Chem. Soc., 124 (2002) 12428-12429.
[21] T. Ohta, T. Tachiyama, K. Yoshizawa, T. Yamabe, T. Uchida, T. Kitagawa, Inorg. Chem., 39 (2000) 4358-4369.
[22] S. Okamoto, L.D. Eltis, Metallomics, 3 (2011) 963-970.
[23] J.A. Kovacs, Chem. Rev., 104 (2004) 825-848.
[24] M. Gennari, B. Gerey, N. Hall, J. Pécaut, M.N. Collomb, M. Rouzières, R. Clérac, M. Orio, C. Duboc, Angew. Chem. Int. Ed., 53 (2014) 5318-5321.
[25] F. Jiang, M.A. Siegler, E. Bouwman, Inorg. Chem. Commun., 94(2018) 53-56.
[26] D. Evans, J. Chem. Soc., (1959) 2003-2005.
[27] G.A. Bain, J.F. Berry, J. Chem. Educ., 85 (2008) 532.
[28] H.E. Van Wart, A. Lewis, H.A. Scheraga, F.D. Saeva, Proc. Natl. Acad. Sci. U.S.A., 70 (1973) 2619-2623.
[29] A.W. Addison, T.N. Rao, J. Reedijk, J. van Rijn, G.C. Verschoor, J. Chem. Soc., Dalton Trans., (1984) 1349-1356.
[30] L.R. Widger, Y. Jiang, A.C. McQuilken, T. Yang, M.A. Siegler, H. Matsumura, P. Moënne-Loccoz, D. Kumar, S.P. De Visser, D.P. Goldberg, Dalton Trans., 43 (2014) 7522-7532.
[31] D. Sellmann, K.P. Peters, F.W. Heinemann, Eur. J. Inorg. Chem., 2004 (2004) 581-590.
[32] U.K. Das, S.L. Daifuku, S.I. Gorelsky, I. Korobkov, M.L. Neidig, J.J. Le Roy, M. Murugesu, R.T. Baker, Inorg. Chem., 55 (2016) 987-997.
[33] A.B.P. Lever, Inorganic electronic spectroscopy, 2nd ed., Elsevier, Amsterdam, the Netherlands, 1968.
[34] B.J. Coe, J.A. Harris, B.S. Brunschwig, I. Asselberghs, K. Clays, J. Garín, J. Orduna, J. Am. Chem. Soc., 127 (2005) 13399-13410.
[35] A. Neuba, R. Haase, W. Meyer-Klaucke, U. Flörke, G. Henkel, Angew. Chem., Int. Ed., 51 (2012) 1714-1718.

[36] G.M. Sheldrick, Acta Crystallogr., Sect. A, 64 (2008) 112-122.
[37] G. te Velde, F.M. Bickelhaupt, E.J. Baerends, C. Fonseca Guerra, S.J.A. Van Gisbergen, J.G. Snijders, T. Ziegler, J. Comput. Chem., 22 (2001) 931-967.
[38] http://www.scm.com/.
[39] M. Swart, A.W. Ehlers, K. Lammertsma, Mol. Phys., 102 (2004) 2467-2474.
[40] A. Klamt, J. Phys. Chem., 99 (1995) 2224-2235.
[41] A. Klamt, G. Schuurmann, J. Chem. Soc. Perk Trans 2, (1993) 799-805.
[42] C.C. Pye, T. Ziegler, Theor. Chem. Acc., 101 (1999) 396-408.
[43] M. Swart, E. Roesler, F.M. Bickelhaupt, Eur. J. Inorg. Chem., (2007) 3646-3654.
[44] L. Noodleman, J. Chem. Phys., 74 (1981) 5737-5743.
[45] L. Noodleman, E.J. Baerends, J. Am. Chem. Soc., 106 (1984) 2316-2327.
[46] F. Jensen, Introduction to Computational Chemistry, 2nd ed., Wiley, Chichester, West Sussex, UK, 2006.